

LETTERS

Signature of high-order azimuthal MHD body modes in sunspot's low atmosphere

Ding Yuan

Centre for mathematical Plasma Astrophysics, Department of Mathematics, KU Leuven, Celestijnenlaan 200B bus 2400, B-3001 Leuven, Belgium; *Ding.Yuan@wis.kuleuven.be*

Received 2015 May 7; accepted 2015 July 7

Abstract The five-minute oscillations inside sunspots appear to be the absorption of the solar p -mode. It is a potential tool to probe a sunspot's sub-structure. We studied the collective properties of five-minute oscillations in the power and phase distribution at the sunspot's umbra-penumbra boundary. The azimuthal distributions of the power and phase of five-minute oscillations enclosing a sunspot's umbra were obtained with images taken with the *Solar Dynamics Observatory*/Atmospheric Imaging Assembly (*SDO/AIA*). The azimuthal modes were quantified with periodogram analysis and justified with significance tests. The azimuthal nodal structures in an approximately axially symmetric sunspot AR 11131 (2010 Dec 08) were investigated. Mode numbers $m = 2, 3, 4, 7, 10$ were obtained in both 1700 Å and 1600 Å bandpasses. The 1600 Å channel also revealed an extra mode at $m = 9$. In the upper atmosphere (304 Å), fewer modes were detected at $m = 3, 4, 7$. The azimuthal modes in the sunspot's low atmosphere could be interpreted as high-order azimuthal MHD body modes. They were detected in the power and phase of the five-minute oscillations in sunspot AR 11131 with *SDO/AIA* data. Fewer modes were detected in the sunspot's upper atmosphere.

Key words: Sun: atmosphere — Sun: UV radiation — Sun: sunspots

1 INTRODUCTION

Sunspot oscillations are one of the most prominently studied magnetohydrodynamic (MHD) wave phenomena in solar physics (e.g., Lites et al. 1992; Bogdan 2000; Bogdan & Judge 2006). The associated MHD seismology is a potential tool to probe the structure of the sunspot's atmosphere (Zhugzhda et al. 1983; Shibasaki 2001; Zhugzhda 2008; Botha et al. 2011; Yuan et al. 2014b,a), and photospheric-coronal magnetic connectivity (Sych et al. 2009; Yuan et al. 2011). Sunspots and their magnetic fields are also excellent test grounds for the theory of MHD waves (Cally 2005; Khomenko & Collados 2006) and for the interaction of acoustic waves with the magnetic field concentrations (Cally et al. 2003; Gordovskyy & Jain 2008). Moreover, sunspot oscillations have appeared to reveal their internal, sub-photospheric structure (Zhugzhda 2008; Jess et al. 2013).

The oscillation power distribution of different periods in a sunspot is non-uniform in both the horizontal and vertical directions (Bogdan & Judge 2006). In particular, three-minute oscillations occupy the sunspot's umbra with the maximum power in the chromosphere (Abdelatif et al. 1986; Reznikova et al. 2012; Yuan et al. 2014b,a). The effect of height inversion occurs in the umbra: a hump in the three-minute oscillation power is normally found at the chromospheric height, however

a power void is usually detected at the photospheric height underneath (Kobanov et al. 2011). In the corona, the three-minute oscillations become propagating slow magnetoacoustic waves and follow magnetic fan structures extending upwards from the sunspot (Yuan & Nakariakov 2012; Kiddie et al. 2012).

On the other hand, in large sunspots, five-minute oscillation power is usually suppressed inside the umbra. The significant power forms a ring-structure at the umbra-penumbra boundary (Nagashima et al. 2007; Sych & Nakariakov 2008; Reznikova et al. 2012; Yuan et al. 2014b,a). The oscillation phase forms patches with alternating positive and negative values along the ring surface (Zhugzhda et al. 2000; Nindos et al. 2002; Sych & Nakariakov 2008). The physical mechanism responsible for such a behavior is still under debate. A solar p -mode acoustic wave is a candidate energy source (Abdelatif et al. 1986). In particular, the interaction of p -modes with the strong magnetic field in the sunspot can lead to the excitation of magnetoacoustic modes (Cally & Bogdan 1997; Cally et al. 2003; Schunker & Cally 2006; Khomenko 2009). Penn & Labonte (1993) suggested that the absorption of p -modes occurs linearly across the sunspot umbra or within a ring surface where the local magnetic field allows an optimized absorption rate. Moreover, the ring surface absorption is favored in theoretical studies (Cally et al. 2003; Schunker & Cally 2006), and the p -mode absorption is optimized at an attack angle at about 30° . The oscillations intermittently localized at the umbra-penumbra boundary can be associated with the “whispering gallery” mode, which is a magnetoacoustic body mode of the sunspot magnetic flux tube with a high azimuthal wavenumber (Zhugzhda et al. 2000). However, as was pointed out in Zhugzhda et al. (2000), there are alternative interpretations, e.g., connection with the random filamentary structure of the magnetic field near the umbra-penumbra boundary. Recently Yuan et al. (2014a) and Yang et al. (2015) detected a significant five-minute oscillation in light bridges, where the magnetic structure is rather different from the penumbral magnetic field. The p -mode absorption theory has to be revised to consider such a scenario.

In this letter, we report observational evidence of high-order azimuthal MHD body modes in a sunspot observed with *Solar Dynamics Observatory*/Atmospheric Imaging Assembly (*SDO*/AIA). The modes have a periodicity of about five minutes, and are observed at the umbra-penumbra boundary. We demonstrate that the power and phase of the five-minute oscillations vary periodically with the azimuthal angle.

2 OBSERVATION

The sunspot considered in this study was situated near 30° latitude in the northern hemisphere. It crossed the central meridian on 2010 Dec 08. It was a large and symmetric sunspot, and the umbra and penumbra were about 10 Mm and 22 Mm in diameter, respectively (Fig. 1). There was a strong magnetic concentration of the south polarity. The north polarity was spread sparsely to the west and north of the sunspot. This sunspot was also studied by Reznikova et al. (2012); Reznikova & Shibasaki (2012); Yuan et al. (2014b).

We used *SDO*/AIA 1700 Å, 1600 Å and 304 Å data (see Lemen et al. 2012; Boerner et al. 2011; Yuan & Nakariakov 2012) for instrumentation, calibration and image flux error analysis, respectively. The images were taken with a time cadence of 24 s/12 s in the UV/EUV channels. We studied sunspot AR 11131, which appeared from 2010 Dec 08 02:30 to 03:30 UT. The sunspot’s low atmosphere was well imaged by the channels that are part of AIA (see Fig. 1). The data sets were prepared with the standard routine *aia_prep.pro* (v4.13). The sunspot center was identified by fitting a contour to the umbral-penumbral boundary (Fig. 1).

3 ANALYSIS

For each data set, the narrowband power maps were prepared at the periods of 2, 2.1, . . . , 20 min with the Pixelised Wavelet Filtering technique (Sych & Nakariakov 2008; Sych et al. 2010).

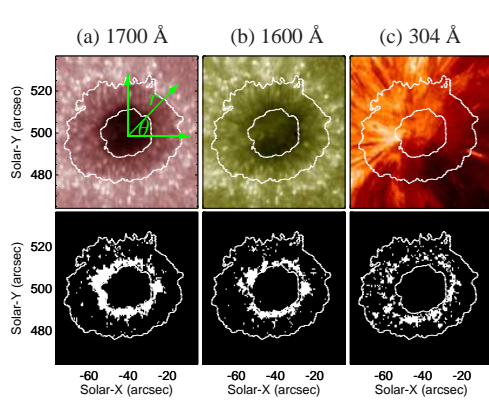


Fig. 1 *Top row*: the AIA intensity images (with a logarithmic scale) illustrate different heights of sunspot AR 11131 (2010 Dec 08). (a) The temperature minimum level (1700 Å), (b) the upper photosphere and transition region (1600 Å) and (c) the chromosphere (304 Å). The polar coordinate system used in this study is shown in (a). *Bottom row*: The corresponding five-minute spatial masks. The inner lines show the boundaries of the umbra and penumbra, determined with the 4500 Å intensity image.

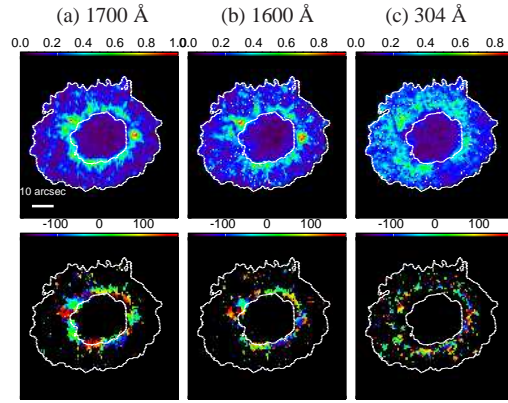


Fig. 2 Five-minute narrow band power maps (*top row*) and the phase maps (*bottom row*). The corresponding AIA bandpasses are 1700 Å (a), 1600 Å (b) and 304 Å (c). A bar in the top left panel shows the scale length of 10 arcsec. The inner curves show the contours separating the umbra and penumbra.

Figure 2 (top row) shows the five-minute power maps. A five-minute spatial mask (Fig. 1, bottom row) was obtained by identifying pixels where the peak period was within 5 ± 0.5 min in the spectra. The phase maps (Fig. 2, bottom row) were obtained by Fourier analyzing the original intensity signals. A similar result was also obtained with the nonlinear least-square fitting technique.

The power and phase maps exhibit nodal patterns along the azimuthal direction (Fig. 2). To quantify this effect, we took the average power and phase along a radial cut at every 5-degree polar angle (2–4 pixels, Figs. 3, 4 and 5, left columns). In this step, we only consider the values within the five-minute spatial mask (Fig. 1). The errors in the parameters were the corresponding standard deviations over the radial direction. One could resolve the azimuthal mode number $m < 36$ in current discretization. The power and phase variations with the polar angle θ were detrended with a running difference of 30 data points with edge wrapping. Then we used a Lomb-Scargle periodogram (Scargle 1982; Horne & Baliunas 1986) to quantify the azimuthal wavenumber or mode number m (Figs. 3, 4 and 5, left columns). The significances of the spectral peaks were assessed with the Horne & Baliunas (1986) test based on the exponential noise distribution and the Fisher randomization test (Linnell Nemec & Nemec 1985) with no bias in the noise distribution (see details in Yuan et al. 2011; Inglis & Nakariakov 2009). In the Horne & Baliunas test, a false alarm probability of 0.05 was chosen. The Fisher randomization test was performed with 1000 permutations in each run, using the PERIOD package (Dhillon et al. 2001). Since both tests can only be applied to the highest peak in the spectrum, the maximum peaks were iteratively removed from the original signal with a harmonic filter (see Ferraz-Mello 1981) to assess the significance of the secondary peaks (Yuan et al. 2011).

4 RESULT

The regions with significant five-minute oscillation power formed a ring structure enclosing the sunspot umbra (Fig. 2). The ring size increased with height, and it may be connected with the ex-

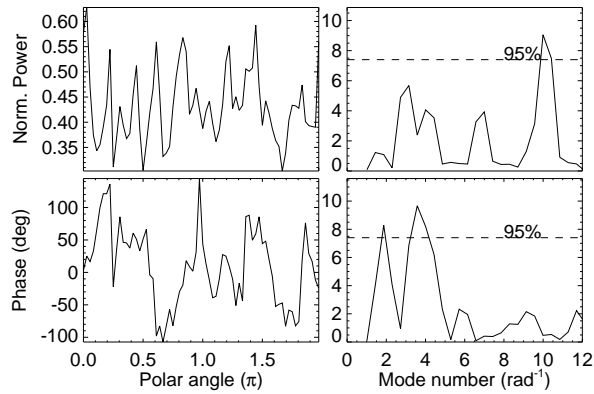


Fig. 3 The azimuthal distributions (*left column*) of the power (*top*) and phase (*bottom*) and the corresponding periodograms (*right column*). The dashed lines in the periodograms mark a confidence level at 95% (or 0.05 in significance level). The analysis was done with the 1700 Å data set.

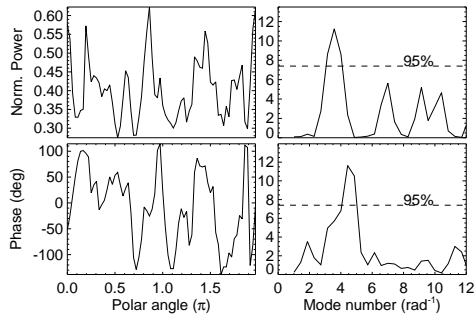


Fig. 4 Same as Fig. 3 but with the 1600 Å data set.

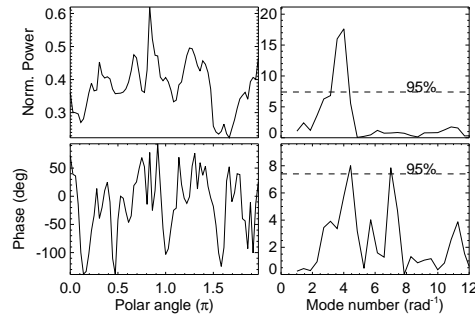


Fig. 5 Same as Fig. 3 but with the 304 Å data set.

panding magnetic field. The oscillation power became more diffused in the upper atmosphere. The power and phase maps exhibited a nodal pattern along the ring, and the typical node size was about 5–8 arcsec. We also investigated three-minute and longer period oscillations, however they did not exhibit steady nodal structures like in the five-minute case (Yuan et al. 2014b).

The power distribution in the 1700 Å bandpass (Fig. 3) exhibited four significant modes at $m = 3.04 \pm 0.75$, 4.06 ± 0.75 , 6.84 ± 0.75 and 10.13 ± 0.75 . The phase distribution gave two significant modes at $m = 1.77 \pm 0.78$ and 3.55 ± 0.75 . All these modes were detected with a low significance value, 0.02 or less (see Table 1).

In the 1600 Å data (Fig. 4), the power distribution presented similar modes as in the 1700 Å data, $m = 3.55 \pm 0.75$, 6.84 ± 0.75 , 10.13 ± 0.75 , and an extra mode at $m = 9.04 \pm 0.75$. In the phase distribution, three modes were detected at $m = 2.03 \pm 0.78$, 3.31 ± 0.78 and 4.56 ± 0.75 . Only $m = 2.03 \pm 0.78$ was lower than the 95% confidence level in the Horne & Baliunas test, but a p -value was assessed to be 0.02 in the randomization test.

In the 304 Å data (Fig. 5) $m = 3.04 \pm 0.75$ and 3.80 ± 0.78 were detected at a low significance level. These modes were also found in the phase distribution ($m = 3.04 \pm 0.78$, 4.34 ± 0.75). Another extra mode of $m = 7.10 \pm 0.75$ was only significantly measured in the phase distribution.

Table 1 Summary of the Detected Modes and Significance Tests

| Bandpass | Mode number | Power distribution | | Phase distribution | |
|----------|-------------|--------------------|--------------|--------------------|--------------|
| | | Peak | Significance | Peak | Significance |
| 1700 Å | $m = 2$ | ... | ... | 1.77 ± 0.78 | ≤ 0.01 |
| | $m = 3$ | 3.04 ± 0.75 | ≤ 0.01 | ... | ... |
| | $m = 4$ | 4.06 ± 0.75 | 0.01 | 3.55 ± 0.75 | 0.02 |
| | $m = 7$ | 6.84 ± 0.75 | 0.02 | ... | ... |
| | $m = 10$ | 10.13 ± 0.75 | ≤ 0.01 | ... | ... |
| 1600 Å | $m = 2$ | ... | ... | $[2.03 \pm 0.78]$ | 0.02 |
| | $m = 3$ | ... | ... | 3.31 ± 0.78 | 0.01 |
| | $m = 4$ | 3.55 ± 0.75 | ≤ 0.01 | ... | ... |
| | $m = 5$ | ... | ... | 4.56 ± 0.75 | ≤ 0.01 |
| | $m = 7$ | 6.84 ± 0.75 | ≤ 0.01 | ... | ... |
| | $m = 9$ | 9.04 ± 0.75 | ≤ 0.01 | ... | ... |
| | $m = 10$ | 10.13 ± 0.75 | ≤ 0.01 | ... | ... |
| 304 Å | $m = 3$ | 3.04 ± 0.75 | ≤ 0.01 | 3.04 ± 0.78 | ≤ 0.01 |
| | $m = 4$ | 3.80 ± 0.78 | ≤ 0.01 | 4.34 ± 0.75 | ≤ 0.01 |
| | $m = 7$ | ... | ... | 7.10 ± 0.75 | 0.01 |

Notes: The errors used 3σ values. The detected values with more than a 0.05 false alarm probability in the Horne & Baliunas test are enclosed in square brackets. p -values less than 0.01 (the lower detection limit) in the applied Fisher's randomization test are denoted ≤ 0.01 .

5 CONCLUSIONS

In this study, the five-minute power ring structure enclosing a sunspot umbra was analyzed with AIA data. It exhibited a stronger power, larger local interaction scale and better nodal structure in the lower atmosphere (1700 Å and 1600 Å, see Fig. 2). These features became more diffused and less clear in the chromosphere (304 Å, see Fig. 2), which implies that the five-minute oscillations may have originated from the photosphere (1700 Å) or even deeper.

Mode numbers $m = 2, 3, 4, 7, 10^1$ were significantly detected in both 1700 Å and 1600 Å bandpasses. An extra mode was found at $m = 9$ in the 1600 Å data. Fewer modes were measured at $m = 3, 4, 7$ in the chromospheric height (304 Å). It is not clear why fewer modes were detected in the higher atmosphere. We speculate that some of the higher modes were not stable or damped very rapidly due to the sharp temperature and density variation in the transition region and chromosphere. Moreover, noise in the data was larger in the higher atmosphere and limited accurate detections.

The azimuthal modes can be interpreted as multi-mode oscillations of a sunspot flux tube (Zhugzhda et al. 2000; Staude 2002), which is an extension of MHD wave modes in a plasma cylinder (Roberts & Webb 1978; Edwin & Roberts 1983). The magnetoacoustic body modes with $m > 1$ confine the maximum modulations to a certain ring surface within the sunspot penumbra. The ring size is specified by the mode number m in the Bessel function of the first kind $J_m(r)$, where r is the distance to the sunspot center. The significant power is confined further away from the sunspot center, as m becomes larger. The modulations to sound speed and Alfvén speed approximately follow the azimuthal profile $\cos(m\theta)$. A theoretical and numerical study is required to fully justify the results.

To directly observe the global multi-mode sunspot oscillation, a time-dependent study of the line intensity, magnetic field and line-of-sight velocity is required. These parameters can be resolved using full Stokes measurements with current ground-based instruments, but the observation interval has to be sufficiently long and cover several cycles of the high-order azimuthal modes.

Acknowledgements DY thanks Prof. V. Nakariakov and Dr. R. Sych for the useful discussion. The data were obtained with the courtesy of NASA/SDO and the AIA, EVE and HMI science teams.

¹ Considering the error bars and noise in different channels, we adopted integer mode number m referring to values obtained in the periodograms in the following discussion.

References

- Abdelatif, T. E., Lites, B. W., & Thomas, J. H. 1986, *ApJ*, 311, 1015
- Boerner, P., Edwards, C., Lemen, J., et al. 2011, *Sol. Phys.*, 316
- Bogdan, T. J. 2000, *Sol. Phys.*, 192, 373
- Bogdan, T. J., & Judge, P. G. 2006, *Royal Society of London Philosophical Transactions Series A*, 364, 313
- Botha, G. J. J., Arber, T. D., Nakariakov, V. M., & Zhugzhda, Y. D. 2011, *ApJ*, 728, 84
- Cally, P. S. 2005, *MNRAS*, 358, 353
- Cally, P. S., & Bogdan, T. J. 1997, *ApJ*, 486, L67
- Cally, P. S., Crouch, A. D., & Braun, D. C. 2003, *MNRAS*, 346, 381
- Dhillon, V. S., et al. 2001, *PERIOD*, A Time-Series Analysis Package Version 5.0 User's Manual
- Edwin, P. M., & Roberts, B. 1983, *Sol. Phys.*, 88, 179
- Ferraz-Mello, S. 1981, *AJ*, 86, 619
- Gordovskyy, M., & Jain, R. 2008, *ApJ*, 681, 664
- Horne, J. H., & Baliunas, S. L. 1986, *ApJ*, 302, 757
- Inglis, A. R., & Nakariakov, V. M. 2009, *A&A*, 493, 259
- Jess, D. B., Reznikova, V. E., Van Doorselaere, T., Keys, P. H., & Mackay, D. H. 2013, *ApJ*, 779, 168
- Khomenko, E. 2009, in *Astronomical Society of the Pacific Conference Series*, 416, 31
- Khomenko, E., & Collados, M. 2006, *ApJ*, 653, 739
- Kiddie, G., De Moortel, I., Del Zanna, G., McIntosh, S. W., & Whittaker, I. 2012, *Sol. Phys.*, 279, 427
- Kobanov, N. I., Kolobov, D. Y., Chupin, S. A., & Nakariakov, V. M. 2011, *A&A*, 525, A41
- Lemen, J. R., Title, A. M., Akin, D. J., et al. 2012, *Sol. Phys.*, 275, 17
- Linnell Nemeč, A. F., & Nemeč, J. M. 1985, *AJ*, 90, 2317
- Lites, B. W., Dunn, R. B., Elmore, D. F., et al. 1992, in *Bulletin of the American Astronomical Society*, 24, 747
- Nagashima, K., Sekii, T., Kosovichev, A. G., et al. 2007, *PASJ*, 59, 631
- Nindos, A., Alissandrakis, C. E., Gelfreikh, G. B., Bogod, V. M., & Gontikakis, C. 2002, *A&A*, 386, 658
- Penn, M. J., & Labonte, B. J. 1993, *ApJ*, 415, 383
- Reznikova, V. E., & Shibasaki, K. 2012, *ApJ*, 756, 35
- Reznikova, V. E., Shibasaki, K., Sych, R. A., & Nakariakov, V. M. 2012, *ApJ*, 746, 119
- Roberts, B., & Webb, A. R. 1978, *Sol. Phys.*, 56, 5
- Scargle, J. D. 1982, *ApJ*, 263, 835
- Schunker, H., & Cally, P. S. 2006, *MNRAS*, 372, 551
- Shibasaki, K. 2001, *ApJ*, 550, 1113
- Staude, J. 2002, *Astronomische Nachrichten*, 323, 317
- Sych, R. A., & Nakariakov, V. M. 2008, *Sol. Phys.*, 248, 395
- Sych, R. A., Nakariakov, V. M., Anfinogentov, S. A., & Ofman, L. 2010, *Sol. Phys.*, 266, 349
- Sych, R., Nakariakov, V. M., Karlicky, M., & Anfinogentov, S. 2009, *A&A*, 505, 791
- Yang, S., Zhang, J., Jiang, F., & Xiang, Y. 2015, *ApJ*, 804, L27
- Yuan, D., & Nakariakov, V. M. 2012, *A&A*, 543, A9
- Yuan, D., Nakariakov, V. M., Chorley, N., & Foullon, C. 2011, *A&A*, 533, A116
- Yuan, D., Nakariakov, V. M., Huang, Z., et al. 2014a, *ApJ*, 792, 41
- Yuan, D., Sych, R., Reznikova, V. E., & Nakariakov, V. M. 2014b, *A&A*, 561, A19
- Zhugzhda, I. D., Locans, V., & Staude, J. 1983, *Sol. Phys.*, 82, 369
- Zhugzhda, Y. D. 2008, *Sol. Phys.*, 251, 501
- Zhugzhda, Y. D., Balthasar, H., & Staude, J. 2000, *A&A*, 355, 347